Arabian Journal for Science and Engineering (2022) 47:3281–3292
https://doi.org/10.1007/s13369-021-06211-4

RESEARCH ARTICLE-ELECTRICAL ENGINEERING

Throughput and Detection Probability of Interweave Cognitive Radio Networks Using Intelligent Reflecting Surfaces

Raed Alhamad[1]

Received: 31 December 2020 / Accepted: 12 September 2021 / Published online: 21 September 2021

Abstract

In this paper, we derive a tight lower bound of the detection probability of the energy detector when intelligent reflecting surface (IRS) are used. The secondary source uses the energy detector to detect primary source activity. There is IRS between primary source and secondary source. The secondary sources compute the energy of the received signal from primary source and reflected on IRS. The proposed spectrum sensing algorithm using IRS offers 15, 21, 27, 33 dB gain with respect to conventional sensing without IRS for a number of reflectors $K = 8, 16, 32, 64$. We also used IRS for data communication between primary source and destination as well as the communication between secondary nodes. The proposed primary and secondary networks of cognitive radio network (CRN) using IRS offer 23, 29, 36, 43, 49 and 56 dB gain with respect to conventional CRN without IRS for a number of reflectors $K = 8, 16, 32, 64, 128, 256$. We show that the use of $N = 20, 10, 5$ symbols in energy detection offers up to 8.5, 7.7 and 4.7 dB gain with respect to a single symbol. We plot the miss detection probability P_{md} versus the false alarm probability P_f. For $K = 16$ reflectors, average SNR per bit $E_b/N_0 = -10\,\mathrm{dB}$ and $P_f = 0.01$, $P_{\mathrm{md}} = 210^{-3}, 710^{-3}, 2.510^{-2}$ when $N = 20, 10, 5$ symbols are used in energy detection, whereas $P_{\mathrm{md}} = 0.45$ when a single symbol is used.

Keywords Cognitive radio networks · Intelligent reflecting surfaces (IRS) · 6G · Spectrum sensing · Energy detection

1 Introduction

Cognitive radio networks (CRN) were suggested to improve the use of frequency bands [1]. There are three possible strategies: In interweave CRN, secondary source is allowed to transmit only when primary user is idle. In underlay cognitive radio networks, secondary source transmits over the same channel as primary source. Secondary source transmits with an adaptive power in order to not cause harmful interference to primary nodes. In overlay CRN, secondary and primary nodes transmit over the same channel and secondary nodes dedicate a part of their power to relay signal to primary nodes and ensure a good quality of service (QoS) in the primary network. The detection probability and throughput of CRN have been extensively studied in [1–5].

In this paper, we suggest a new spectrum sensing algorithm where the energy detector uses a signals obtained from reflections on intelligent reflecting surface (IRS) [6–8]. The phases of IRS are optimized so that all reflections have a null phase at the receiver [9–14]. IRS can be used in non-orthogonal multiple access (NOMA) systems as well as millimeter wave or free-space optical (FSO) communications [15–18]. A hardware and practical implementation of IRS was discussed in [19,20]. The phase shifts of IRS reflectors can be continuous or quantized [21,22]. To the best of our knowledge, the use of IRS in the spectrum sensing process with multiple symbols was not yet suggested to improve the detection probability.

2 Related Work

The false alarm and detection probabilities of the energy detector using a single symbol and intelligent reflecting surfaces were recently derived in [23]. The secondary throughput using IRS was derived in [23] as the product of the secondary user transmit probability and the transmission rate. The packet error probability was not studied in [23]. In [24], the transmitted power is minimized for CRN using IRS. The

✉ Raed Alhamad
ralhamad@seu.edu.sa

1 Saudi Electronic University, Riyadh, Kingdom of Saudi Arabia

minimization has been performed under the constraint that the signal to interference plus noise ratio (SINR) is larger than a predetermined threshold for all users. The spectral and energy efficiencies of CRN using IRS were maximized in [25,26]. The achievable weighted sum rate was maximized in [27]. The achievable rate of secondary users was maximized in [28] subject to a total transmit power constraint. Optimal resource allocation for CRN using IRS was proposed in [28]. Vertical and robust beamforming has been proposed to improve the performance of CRN using IRS [29,30]. The physical layer security of CRN using IRS was studied in [31,32] in order to maximize the secrecy rate.

The main innovation and contributions of the paper are:

- We suggest the use of IRS in the spectrum sensing process. The energy detector uses N symbols. The use of $N = 20, 10, 5$ symbols in energy detection offers up to 8.5, 7.7 and 4.7 dB gain with respect to $N = 1$ as considered in [23]. We derive the detection probability P_d and the miss detection probability of the energy detector using intelligent reflecting surface (IRS). The proposed spectrum sensing algorithm using IRS offers 15, 21, 27, 33 dB gain with respect to conventional sensing without IRS [1-5] for a number of reflectors $K = 8, 16, 32, 64$.

- We derive the throughput of the primary and secondary networks of CRN using interweave transmission technique where secondary source is allowed to transmit only when primary source is idle. The proposed primary and secondary networks of CRN using IRS offer 23, 29, 36, 43, 49 and 56 dB gain with respect to conventional CRN without IRS [1-5] for a number of reflectors $K = 8, 16, 32, 64, 128, 256$.

- We plot the miss detection probability $P_{\text{md}} = 1 - P_d$ versus the false alarm probability P_f. For $K = 16$ reflectors, average SNR per bit $E_b/N_0 = -10$ dB and $P_f = 0.01$, $P_{\text{md}} = 210^{-3}, 710^{-3}, 2.510^{-2}$ when $N = 20, 10, 5$ symbols are used in energy detection, whereas $P_{\text{md}} = 0.45$ when a single symbol is used ($N = 1$) as studied in [23].

The paper contains eight sections. The system model is presented in Sect. 3. Section 4 derives a tight lower bound of detection probability of the energy detector using intelligent reflecting surfaces. Sections 5–6 derive the throughput in primary and secondary networks using IRS. Section 7 discusses the obtained results. Section 8 summarizes the obtained results. Section 9 concludes the paper.

3 System Model

Figure 1 shows the system model with a primary source and destination (P_S and P_D), a secondary source and destination (S_S and S_D). We consider interweave cognitive radio networks (CRN) where S_S performs spectrum sensing and is allowed to transmit only when P_S is idle. We assume that P_S is active with probability p_a. S_S uses the energy detector (ED) to measure the energy of received signal and will detect P_S is the measured energy E is larger than threshold T. Intelligent reflecting surfaces (IRSs) are placed between all nodes to improve the throughput and detection probability as all reflections have the same phase at the secondary and primary destination. Besides, IRSs are placed between P_S and S_S so that the spectrum sensing is based on received signals originating from all K reflections.

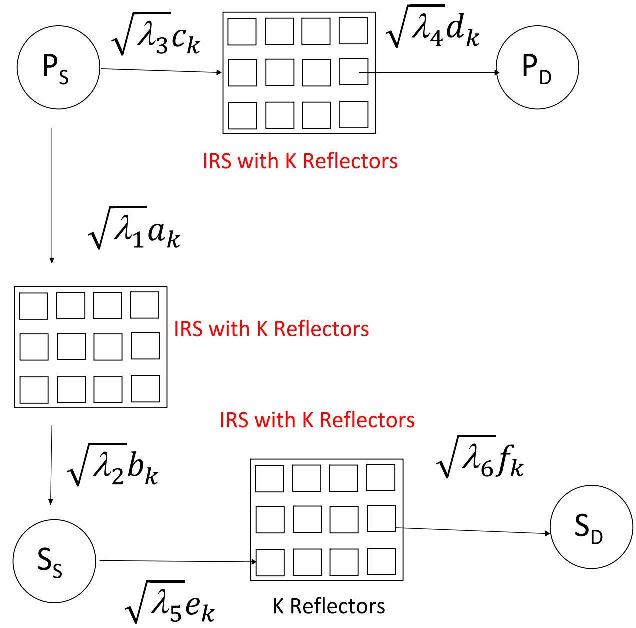

Fig. 1 System model: interweave CRN using intelligent reflecting surface (IRS)

4 Spectrum Sensing Using Intelligent Reflecting Surface (IRS)

Spectrum sensing is performed at S_S to detect P_S activity. The energy detector is used at S_S to detect if P_S is active or idle. S_S receives K reflected signals on IRS. Let $\sqrt{\lambda_1}a_k$ the channel coefficient between P_S and k-th reflector of IRS, $\lambda_1 = \frac{\text{PAL}}{d_1^{\beta}}$ is the average power of channel gain, PAL $= 1$ is the path loss at reference distance d_0, $d_1 = \frac{d_1^{\text{eff}}}{d_0}$ is the normalized distance between P_S and IRS, d_0 is a reference distance in meters, d_1^{eff} is the effective distance in meters between P_S and IRS and β is the path loss exponent. Therefore, d_1 is a normalized distance without unit. The same model is used for all other links with PAL $= 1$ and all other distances $d_i, i = 1, \ldots, 6$ are also normalized. For Rayleigh channels, a_k is a zero-mean complex Gaussian random variable (R.V.) with module $g_k = |a_k|$ and phase ϕ_k: $a_k = g_k e^{-j\phi_k}$. g_k is Rayleigh distributed with mean $\frac{\sqrt{\pi}}{2}$ and unit second order moment. Let $\sqrt{\lambda_2}b_k$ be the channel coefficient between k-th

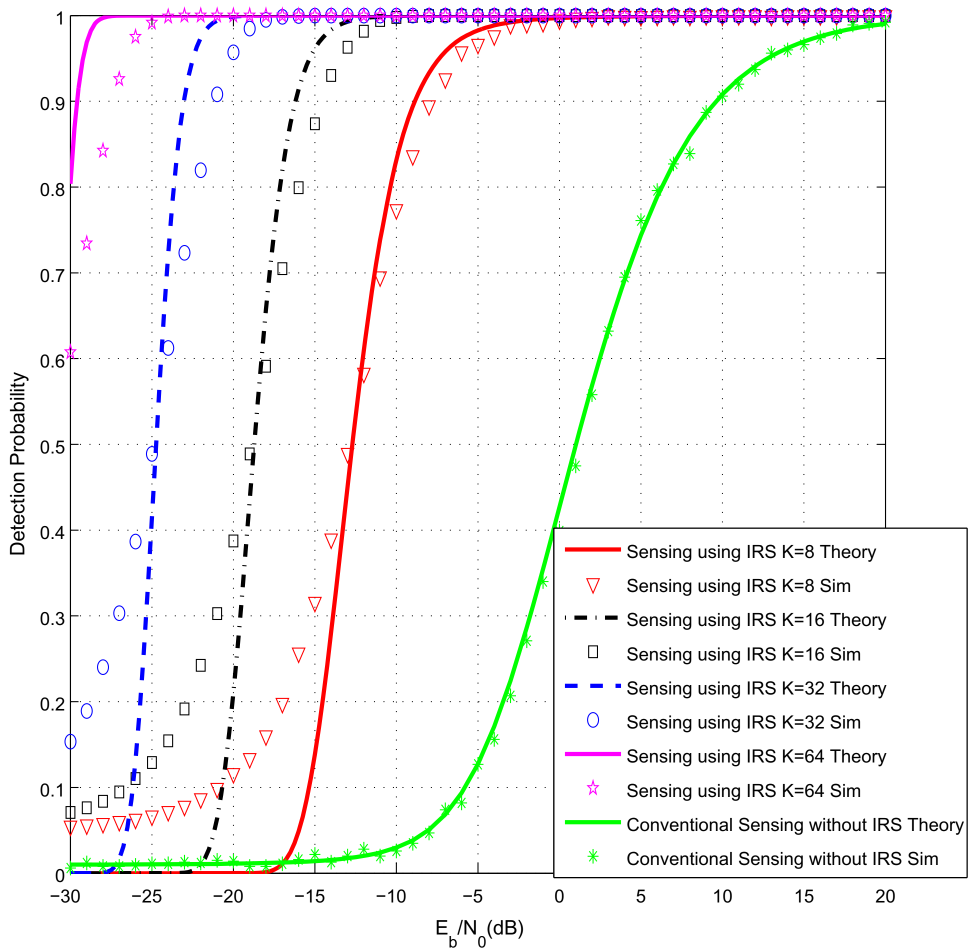

Fig. 2 Detection probability when IRS is deployed as a reflector

reflector of IRS and S_S. $\lambda_2 = \frac{1}{d_2^{\beta}}$ where d_2 is the normalized distance between IRS and S_S. We denote by $b_k = h_k e^{-j\theta_k}$, $h_k = |b_k|$ is the absolute value of b_k and θ_k is the phase. h_k is Rayleigh distributed with mean $\frac{\sqrt{\pi}}{2}$ and unit second-order moment.

Let ζ_k be the phase shift induced by k-th IRS reflector. ζ_k is adjusted so that all K reflections have the same phase at S_S:

$$\zeta_k = \phi_k + \theta_k. \tag{1}$$

The received signal at S_S is written as:

$$r_l^{S_S} = s_l^{P_S}\sqrt{2E_{P_S}\lambda_1\lambda_2}\sum_{k=1}^{K} a_k b_k e^{j\zeta_k} + n_l^{S_S}, \tag{2}$$

where $s_l^{P_S}$ is the l-th transmitted symbol by P_S, $1 \le l \le N$, N is the number of symbols used by the energy detector in the spectrum sensing process, E_{P_S} is the transmitted energy per symbol of node P_S, $n_l^{S_S}$ is zero-mean Gaussian noise with variance $2N_0$.

Using (1) and (2), we obtain

$$r_l^{S_S} = s_l^{P_S}\sqrt{2E_{P_S}\lambda_1\lambda_2}A + n_l^{S_S}, \tag{3}$$

where

$$A = \sum_{k=1}^{K} g_k h_k. \tag{4}$$

Secondary source S_S computes the energy E of received signal $r_l^{S_S}$ to detect P_S activity:

$$E = \frac{\sum_{l=1}^{N}|r_l^{S_S}|^2}{N_0} = \frac{2N\lambda_1\lambda_2 E_{P_S}}{N_0}A^2 + \frac{\sum_{l=1}^{N}|n_l^{S_S}|^2}{N_0} \tag{5}$$

For a fixed value of channel gains, i.e., fixed value of A, E is the sum of $2N$ Gaussian R.V. with unit variance and non-centrality parameter (NCP):

$$NCP = 2N\Gamma_{P_S S_S}, \tag{6}$$

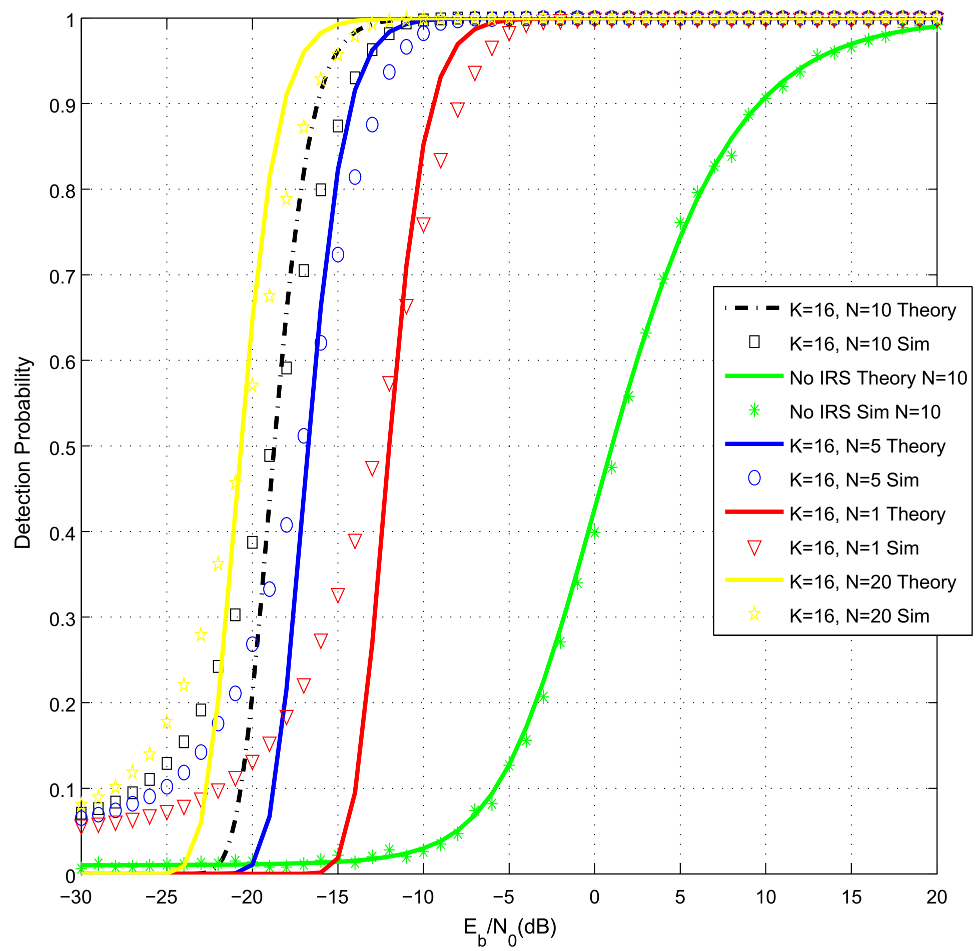

Fig. 3 Detection probability when IRS is deployed as a reflector for different numbers of symbols N used in energy detection: $K = 16$

where $\Gamma_{P_S S_S}$ is the signal-to-noise ratio (SNR) at S_S defined as [33]:

$$\Gamma_{P_S S_S} = \frac{\lambda_1 \lambda_2 E_{P_S} A^2}{N_0} = ASNR \times A^2, \tag{7}$$

where

$$ASNR = \frac{\lambda_1 \lambda_2 E_{P_S}}{N_0}. \tag{8}$$

Using the central limit theorem (CLT), A is approximated by a Gaussian R.V. with mean $m_A = \frac{K\pi}{4}$ and variance $\sigma_A^2 = K(1 - \frac{\pi^2}{16})$. The conditioned detection probability (DP) is equal to

$$P_d(\Gamma_{P_S S_S}) = Q_N(\sqrt{NCP}, \sqrt{T}) = Q_N(\sqrt{2N\Gamma_{P_S S_S}}, \sqrt{T}), \tag{9}$$

where T is the ED threshold and $Q_N(.,.)$ is the generalized Macum Q-function.

The average detection probability (ADP) is computed as:

$$P_d = \int_0^{+\infty} P_d(x) f_{\Gamma_{P_S S_S}}(x) \mathrm{d}x, \tag{10}$$

where $f_{\Gamma_{P_S S_S}}(x)$ is the probability density function (PDF) of $\Gamma_{P_S S_S}$.

$\Gamma_{P_S S_S}$ is a non-central Chi-square R.V. with PDF: [33]

$$f_{\Gamma_{P_S S_S}}(x) = \frac{e^{-\frac{m_A^2}{2\sigma_A^2}}}{2ASNR\sigma_A^2} \left(\frac{x}{m_A^2 ASNR}\right)^{-0.25} e^{-\frac{x}{2\sigma_A^2 ASNR}} I_{-0.5}\left(\sqrt{\frac{m_A^2 x}{\sigma_A^4 ASNR}}\right) \tag{11}$$

The average miss detection probability is equal to

$$P_{\text{md}} = \int_0^{+\infty} [1 - P_d(x)] f_{\Gamma_{P_S S_S}}(x) \mathrm{d}x, \tag{12}$$

We use the tight upper bound derived in [34]

$$P_{\text{md}} < F_{\Gamma_{P_S S_S}}(w_0), \tag{13}$$

where $F_{\Gamma_{P_S S_S}}(w_0)$ is the cumulative distribution function (CDF) of SNR given by

$$F_{\Gamma_{P_S S_S}}(w_0) = 1 - Q_{0.5}\left(\frac{m_A}{\sigma_A}, \sqrt{\frac{x}{ASNR\sigma_A^2}}\right), \tag{14}$$

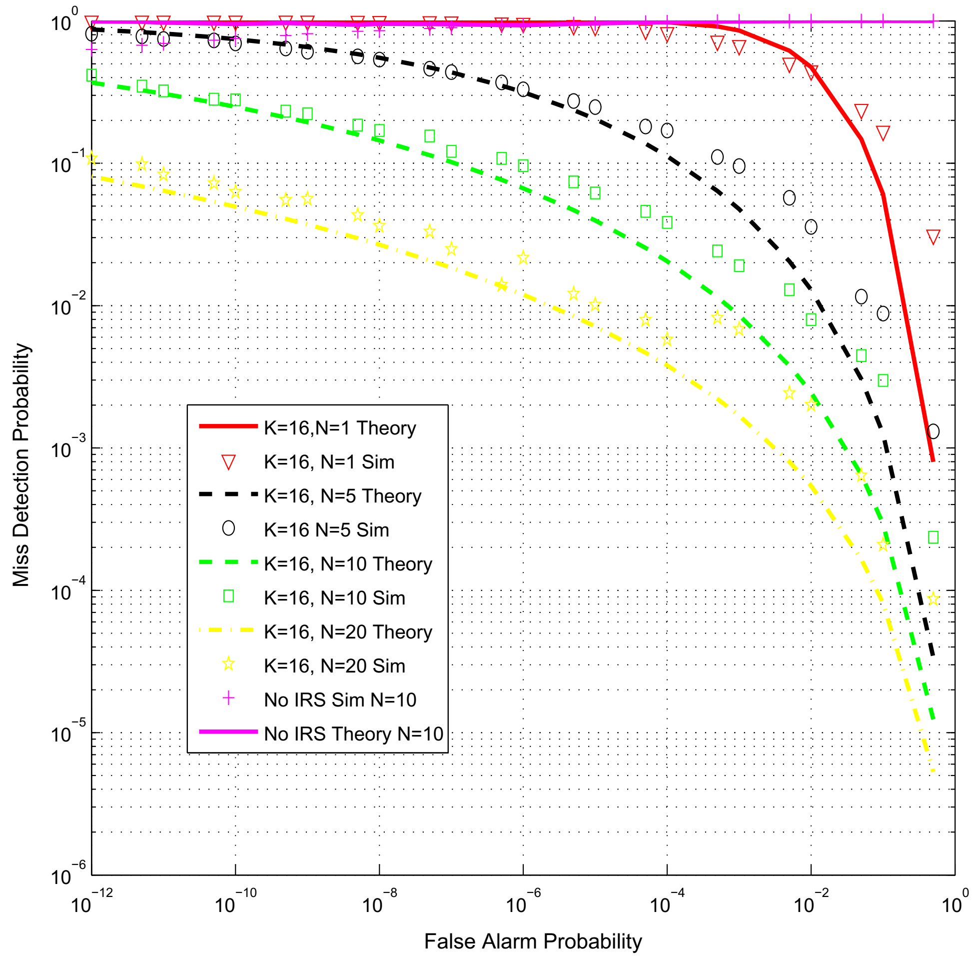

Fig. 4 Miss detection probability versus false alarm probability

and w_0 is water-fall threshold defined as [34]:

$$w_0 = \int_0^{+\infty} [1 - P_d(x)]\mathrm{d}x. \tag{15}$$

We deduce a tight lower bound of detection probability

$$P_d > 1 - F_{\Gamma_{P_S s_S}}(w_0) = Q_{0.5}\left(\frac{m_A}{\sigma_A}, \sqrt{\frac{x N_0}{E_{P_S}\lambda_1\lambda_2\sigma_A^2}}\right). \tag{16}$$

5 IRS Deployed in the Primary Network

IRSs are deployed in the primary network between P_S and P_D. Let $\sqrt{\lambda_3}c_k$ be the channel coefficient between P_S and k-th reflector of IRS. $\lambda_3 = \frac{1}{d_3^\beta}$ where d_3 is the normalized distance between P_S and IRS. We can write $c_k = i_k e^{-j\eta_k}$ where $i_k = |c_k|$ is the absolute value of c_k and η_k is the phase of c_k. i_k is Rayleigh distributed with mean $\frac{\sqrt{\pi}}{2}$ and unit second-order moment.

Let $\sqrt{\lambda_4}d_k$ be the channel coefficient between k-th reflector of IRS and P_D. $\lambda_4 = \frac{1}{d_4^\beta}$ where d_4 is the normalized distance between IRS and P_D. We can write $d_k = j_k e^{-j\mu_k}$ where $j_k = |d_k|$ is the absolute value of d_k and μ_k is the phase of d_k. j_k is Rayleigh distributed with mean $\frac{\sqrt{\pi}}{2}$ and unit second-order moment.

The phase of k-th reflector of IRS is adjusted so that all reflections have the same phase at P_D:

$$v_k = \eta_k + \mu_k. \tag{17}$$

The received signal at P_D is equal to

$$r_l^{P_D} = s_l^{P_S}\sqrt{2E_{P_S}\lambda_3\lambda_4}\sum_{k=1}^{K} c_k d_k e^{j v_k} + n_l^{P_D} \tag{18}$$

where $n_l^{P_D}$ is a zero-mean Gaussian noise with variance $2N_0$.

Using (17), we obtain

$$r_l^{P_D} = s_l^{P_S}\sqrt{2E_{P_S}\lambda_3\lambda_4}B + n_l^{P_D} \tag{19}$$

Fig. 5 Primary throughput for 64QAM modulation when IRS is deployed as a reflector

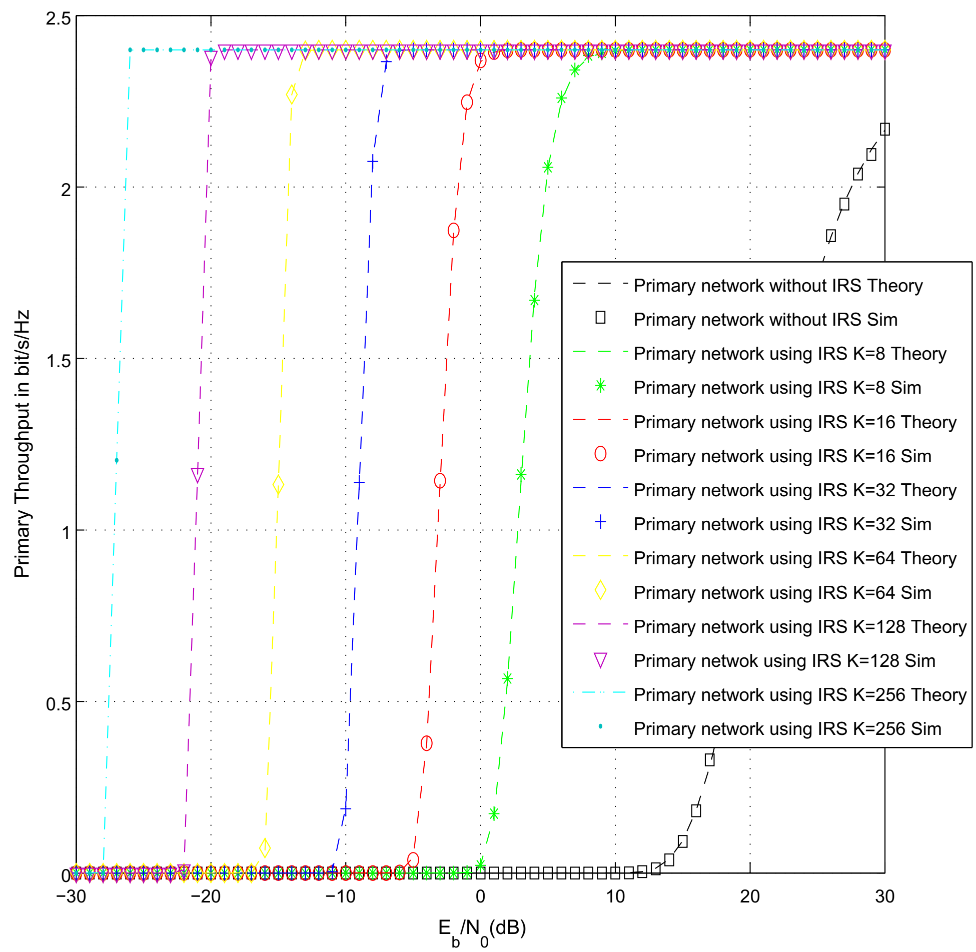

where

$$B = \sum_{k=1}^{K} i_k j_k. \tag{20}$$

Using the CLT, B is approximated by a Gaussian R.V. with mean $m_A = \frac{K\pi}{4}$ and variance $\sigma_A^2 = K(1 - \frac{\pi^2}{16})$. Here, K is the number of IRS reflectors between P_S and P_D that can be different from the number of reflectors between P_S and S_S.

The SNR at P_D is equal to

$$\Gamma_{P_S P_D} = \frac{E_{P_S}\lambda_3\lambda_4}{N_0}B^2. \tag{21}$$

Using the CLT, $\Gamma_{P_S P_D}$ is approximated by a non-central Chi-square distribution with one degree of freedom and CDF:

$$F_{\Gamma_{P_S P_D}}(x) = 1 - Q_{0.5}\left(\frac{m_B}{\sigma_B}, \sqrt{\frac{xN_0}{\lambda_3\lambda_4 E_{P_S}\sigma_A^2}}\right). \tag{22}$$

The packet error probability (PEP) at P_D is tightly upper bounded using the CDF of SNR [35]

$$PEP^{P_D} < F_{\Gamma_{P_S P_D}}(T_0). \tag{23}$$

where T_0 is a water-fall threshold defined as:

$$T_0 = \int_0^{+\infty} 1 - [1 - SEP(x)]^L \mathrm{d}x, \tag{24}$$

where L is packet length and $SEP(x)$ is the symbol error probability (SEP) of M-quadrature amplitude modulation (QAM) defined as [33]:

$$SEP(x) = 2\left(1 - \frac{1}{\sqrt{M}}\right) erfc\left(\sqrt{x\frac{3\log_2(M)}{2(M-1)}}\right), \tag{25}$$

The throughput at P_D is computed as:

$$Thr^{P_D} = p_a log_2(M)[1 - PEP^{P_D}]. \tag{26}$$

where p_a is the probability that P_S is active.

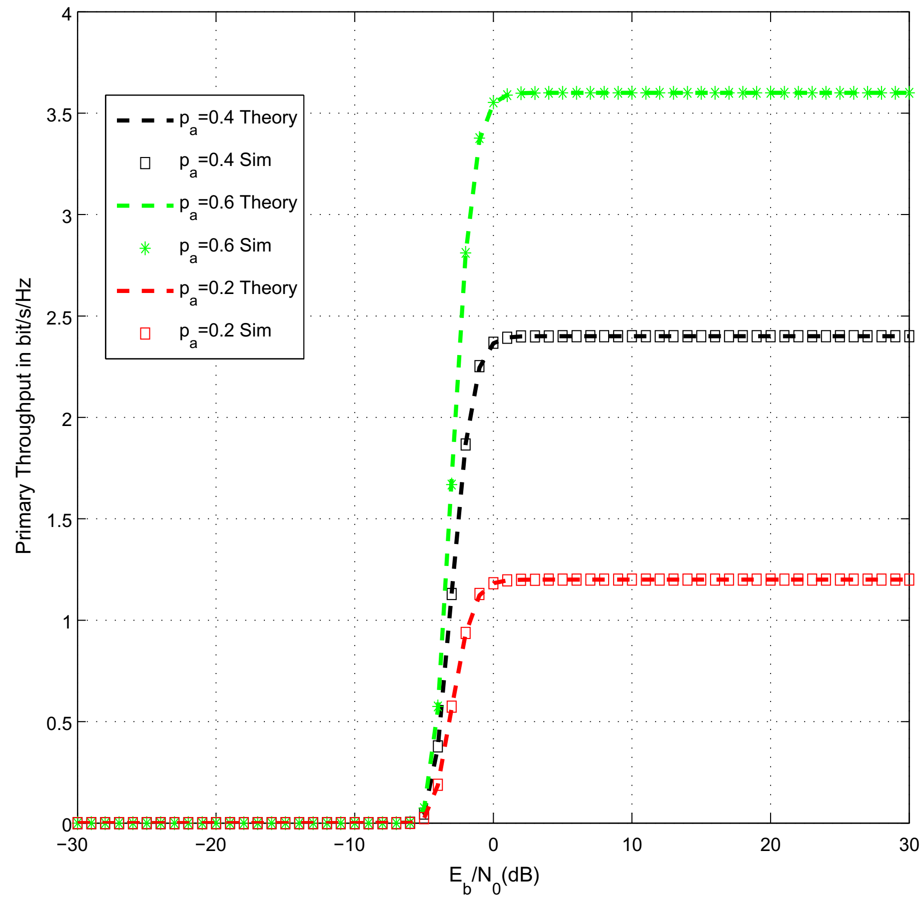

Fig. 6 Primary throughput for 64QAM modulation for different values of p_a; $K = 16$

6 IRS Deployed in the Secondary Network

IRSs are deployed in the secondary network between S_S and S_D. Let $\sqrt{\lambda_5}e_k$ be the channel coefficient between S_S and k-th reflector of IRS. $\lambda_5 = \frac{1}{d_5^\beta}$ where d_5 is the normalized distance between S_S and IRS. We can write $e_k = l_k e^{-jm_k}$ where $l_k = |e_k|$ is the absolute value of e_k and m_k is the phase of e_k. l_k is Rayleigh distributed with mean $\frac{\sqrt{\pi}}{2}$ and unit second-order moment.

Let $\sqrt{\lambda_6}f_k$ be the channel coefficient between k-th reflector of IRS and S_D. $\lambda_6 = \frac{1}{d_6^\beta}$ where d_6 is the normalized distance between IRS and S_D. We can write $f_k = o_k e^{-jp_k}$ where $o_k = |f_k|$ is the absolute value of f_k and p_k is the phase of f_k. o_k is Rayleigh distributed with mean $\frac{\sqrt{\pi}}{2}$ and unit second-order moment.

The phase of k-th reflector of IRS is adjusted so that all reflections arrive with the same phase at S_D:

$$w_k = m_k + p_k. \tag{27}$$

The received signal at S_D is equal to

$$r_l^{S_D} = s_l^{S_S}\sqrt{2E_{S_S}\lambda_5\lambda_6}\sum_{k=1}^{K} e_k f_k e^{jw_k} + n_l^{S_D} \tag{28}$$

where $s_l^{S_S}$ is the l-th transmitted symbol by S_S, E_{S_S} is the transmitted energy per symbol of secondary source S_S and $n_l^{P_D}$ is a zero-mean Gaussian noise with variance $2N_0$.

Using (27), we obtain

$$r_l^{S_D} = s_l^{S_S}\sqrt{2E_{S_S}\lambda_5\lambda_6}C + n_l^{S_D} \tag{29}$$

where

$$C = \sum_{k=1}^{K} l_k o_k. \tag{30}$$

Using the CLT, C is approximated by a Gaussian R.V. with mean $m_C = \frac{K\pi}{4}$ and variance $\sigma_C^2 = K(1 - \frac{\pi^2}{16})$.

The SNR at S_D is equal to

$$\Gamma_{S_S S_D} = \frac{E_{S_S}\lambda_5\lambda_6}{N_0}C^2. \tag{31}$$

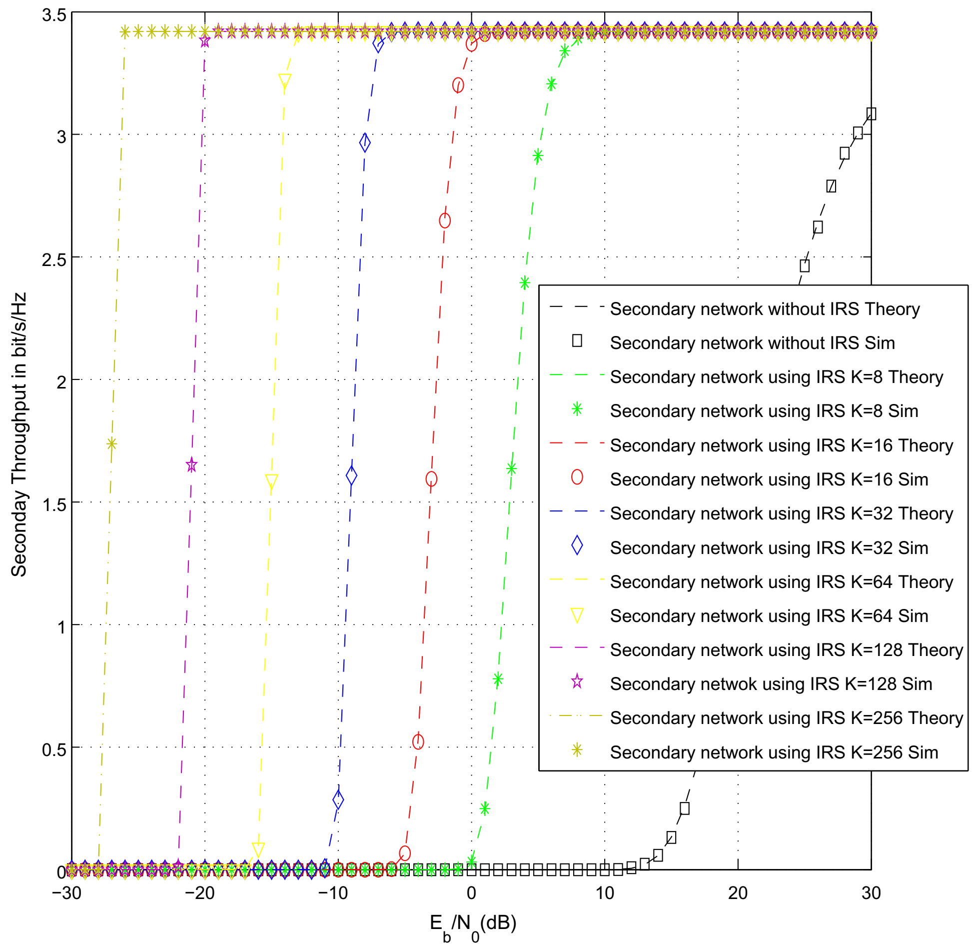

Fig. 7 Secondary throughput for 64QAM modulation when IRS is deployed as a reflector

Using the CLT, $\Gamma_{S_S S_D}$ is approximated by a non-central Chi-square distribution with one degree of freedom and CDF:

$$F_{\Gamma_{S_S S_D}}(x) = 1 - Q_{0.5}\left(\frac{m_C}{\sigma_C}, \sqrt{\frac{x N_0}{\lambda_5 \lambda_6 E_{S_S} \sigma_C^2}}\right). \tag{32}$$

The packet error probability (PEP) at S_D is tightly upper bounded using the CDF of SNR [35]

$$PEP^{S_D} < F_{\Gamma_{S_S S_D}}(T_0). \tag{33}$$

where T_0 is defined in (24).

The throughput at S_D is computed as:

$$Thr^{S_D} = [1 - p_a][1 - P_f] log_2(M)[1 - PEP^{S_D}]. \tag{34}$$

where P_f is the false detection probability defined as:

$$P_f = \frac{\Gamma(N, \frac{T}{2})}{\Gamma(N)}, \tag{35}$$

where $\Gamma(.,.)$ is the incomplete Gamma function, $\Gamma(.)$ is the Gamma function, N is the number of symbols used by the energy detector, and T is the detection threshold.

7 Theoretical and Simulation Results

We have made simulations using MATLAB software for a fixed false alarm probability $\overline{P_f} = 0.05$ in Figs. 2, 3, 7 and 8 by setting the detection threshold as follows:

$$T = 2\Gamma^{-1}(N, \overline{P_f}\Gamma(N)) \tag{36}$$

We used $N = 10$ symbols for spectrum sensing using the energy detector in Fig. 2. The normalized distance between P_S and IRS (placed between P_S and S_S) is $d_1 = 1$. The normalized distance between IRS and S_S is $d_2 = 1.1$. The normalized distance between P_S and IRS of primary network is $d_3 = 1$. The normalized distance between IRS of primary network and P_D is $d_4 = 1.3$. The normalized distance between S_S and IRS of secondary network is $d_5 = 1.3$. The normalized distance between IRS of secondary network and S_D is $d_6 = 1$. The path loss exponent is $\beta = 3$.

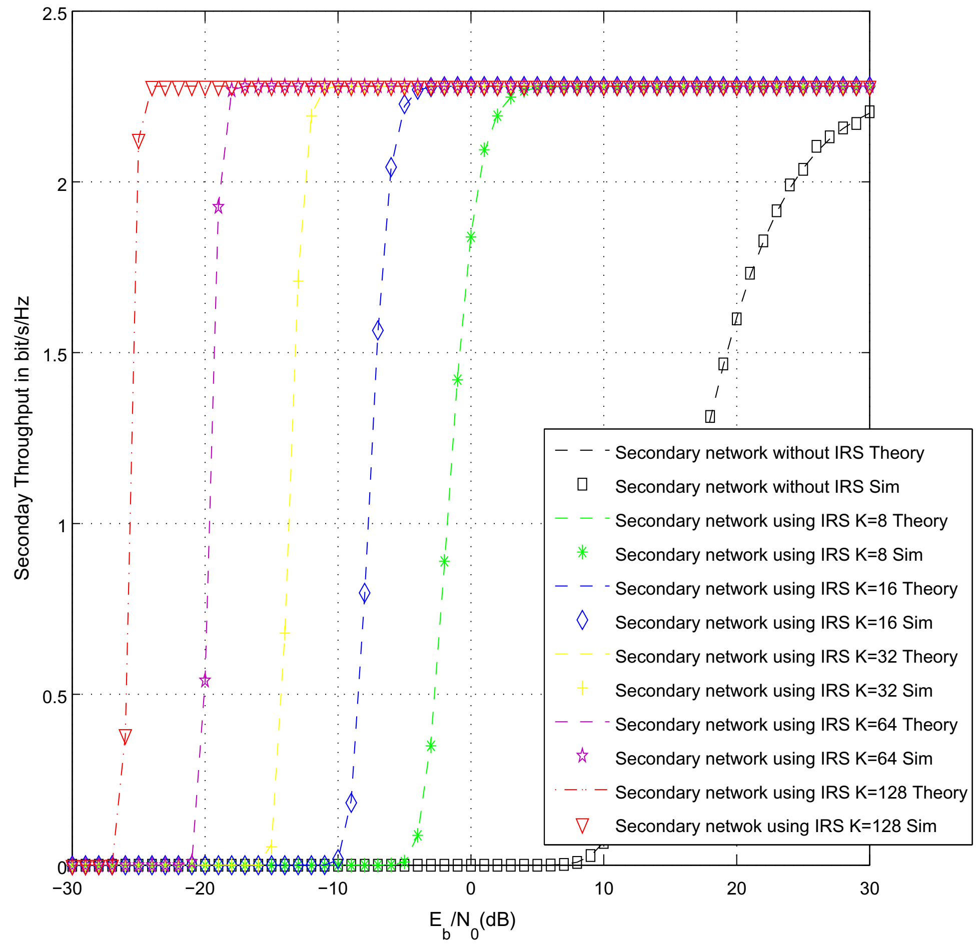

Fig. 8 Secondary throughput for 16QAM modulation when IRS is deployed as a reflector

Figure 2 compares the detection probability at S_S when using IRS to conventional spectrum sensing algorithms [1-5]. To measure the detection probability, we did 10 000 Monte Carlo simulations. We plotted the detection probability versus E_b/N_0 where $E_b = \frac{E_s}{log_2(M)}$ is the transmitted energy per bit and M is the size of the constellation. $E_s = PT_s$ is the transmitted energy per symbol, T_s is the symbol duration and P is the power of primary source P_S. We have fixed the value of N_0 and varied the transmitted power P to obtain different values of E_b/N_0. We observe the proposed spectrum sensing algorithm using IRS offers 15, 21, 27, 33 dB gain with respect to conventional sensing without IRS [1-5] for a number of reflectors $K = 8, 16, 32, 64$. The simulation results are close to the derived theoretical ones.

Figure 3 shows the detection probability versus the average SNR per bit for $K = 16$ reflectors and the same parameters as Fig. 2. Figure 3 shows that the use of $N = 20, 10, 5$ symbols in energy detection offers up to 8.5, 7.7 and 4.7 dB gain with respect to a single symbol, $N = 1$, as considered in [23].

Figure 4 depicts the miss detection probability $P_{\mathrm{md}} = 1 - P_d$ versus the false alarm probability P_f for average SNR per bit $E_b/N_0 = -10\,\mathrm{dB}$. When there is no IRS, $P_{\mathrm{md}} = 1$ as the average SNR per bit is very low. For $P_f = 0.01$, $P_{\mathrm{md}} = 210^{-3}, 710^{-3}, 2.510^{-2}$ when $N = 20, 10, 5$ symbols are used in energy detection, whereas $P_{\mathrm{md}} = 0.45$ when a single symbol is used $N = 1$ as studied in [23].

Figure 5 compares the throughput at primary destination for 64QAM modulations when IRS are used to conventional CRN without IRS [1-5]. We have measured the packet error rate (PER) to deduce the throughput. Simulations have been performed until 500 packets are erroneously received. The primary user is active with probability $p_a = 0.4$. The proposed primary network of CRN using IRS offers 23, 29, 36, 43, 49 and 56 dB gain with respect to conventional CRN without IRS [1-5] for a number of reflectors $K = 8, 16, 32, 64, 128, 256$.

Figure 6 depicts the primary throughput for 64QAM modulation, $K = 16$ reflectors and the same parameters as Fig. 5. We have varied the value of the probability that primary user is active $p_a = 0.6, 0.4, 0.2$. Obviously, as p_a increases, the primary throughput increases.

Figures 7, 8 show the throughput at the secondary destination for 64-QAM and 16-QAM modulation using IRS.

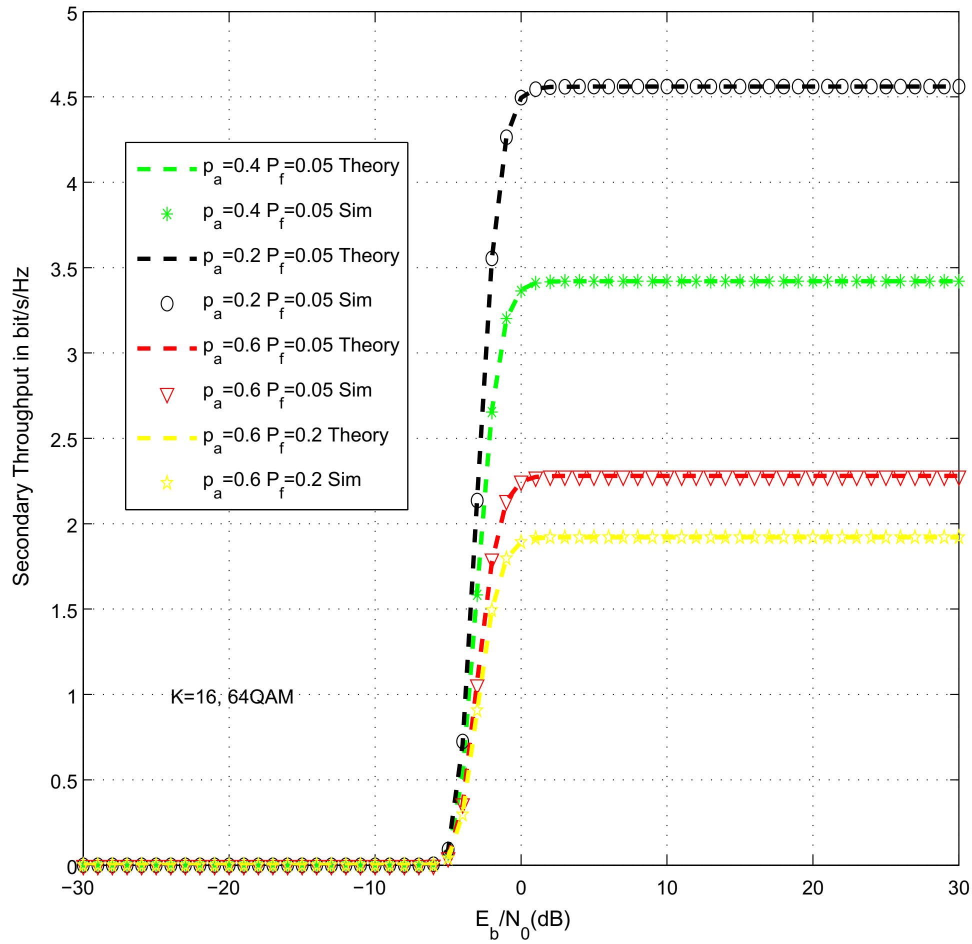

Fig. 9 Secondary throughput for 64QAM modulation for different values of p_a and P_f: $K = 16$

The proposed secondary network of CRN using IRS offers 23, 29, 36, 43, 49 and 56 dB gain with respect to conventional CRN without IRS [1-5] for a number of reflectors $K = 8, 16, 32, 64, 128, 256$.

Figure 9 depicts the secondary throughput for 64QAM modulations and the same parameters as Fig. 7. We plotted the secondary throughput for $K = 16$ reflectors and different values of the probability that primary user is active $p_a = 0.6, 0.4, 0.2$. We also varied the false alarm probability $P_f = 0.05, 0.2$. The secondary throughput decreases as the false alarm probability P_f increases or the probability that primary user is active p_a increases.

8 Discussion on the Obtained Results

In this paper, we have shown that the use of IRS allows to increase the detection probability of the energy detector. The proposed spectrum sensing algorithm using IRS offers 15, 21, 27, 33 dB gain with respect to conventional sensing without IRS [1-5]. We have also shown that the use of $N = 20, 10, 5$ symbols during energy detection offers up to 8.5, 7.7 and 4.7 dB gain with respect to a single symbol, $N = 1$, as considered in [23]. We also plotted the miss detection probability P_{md} versus the false alarm probability P_f. For $K = 16$ reflectors, average SNR per bit $E_b/N_0 = -10$ dB and $P_f = 0.01$, $P_{\text{md}} = 210^{-3}, 710^{-3}, 2.510^{-2}$ when $N = 20, 10, 5$ symbols are used in energy detection, whereas $P_{\text{md}} = 0.45$ when a single symbol is used. IRS allows also to increase the throughput of primary and secondary networks. The proposed primary and secondary networks of CRN using IRS offer 23, 29, 36, 43, 49 and 56 dB gain with respect to conventional CRN without IRS [1-5] for a number of reflectors $K = 8, 16, 32, 64, 128, 256$.

9 Conclusions and Perspectives

In this paper, we suggested a new spectrum sensing algorithm using intelligent reflecting surface (IRS). We derived a tight lower bound of detection probability of the energy detector using IRS. We observe the proposed spectrum sensing algorithm using IRS offers 15, 21, 27, 33 dB gain with respect to conventional sensing without IRS [1-5] for a number of reflectors $K = 8, 16, 32, 64$. We also used IRS for data communication between primary source and destination as well as the communication between secondary nodes. The proposed primary and secondary networks of CRN using IRS offer 23, 29, 36, 43, 49 and 56 dB gain with respect to conventional CRN without IRS [1-5] for a number of reflectors $K = 8, 16, 32, 64, 128, 256$. As a perspective, it will be interesting to derive the detection probability, primary and secondary throughput when the primary source and secondary source harvest energy using radio frequency signals, solar energy or wind.

References

1. Bryan G.; Pourranjbar A.; Kaddoum G.: Collaborative spectrum sensing in tactical wireless networks. ICC—IEEE International Conference on Communications (ICC) (2020)
2. Xiangyue M.; Hazer I.; Brian K.: End-to-end deep learning-based compressive spectrum sensing in cognitive radio networks. ICC 2020–2020 IEEE International Conference on Communications (ICC), 21–24 (2020)
3. Runze, W.; Mou, W.; Luokai, H.; Haijun, W.: Energy-efficient cooperative spectrum sensing scheme based on spatial correlation for cognitive. IEEE Access Internet Things **8**(1), 139501–139511 (2020)
4. Mehran, G.; Fakharzadeh, M.: A fast soft decision algorithm for cooperative spectrum sensing. IEEE Trans. Circuits Syst. II Exp. Briefs **68**(1), 241–245 (2020)
5. Patel, D.; Brijesh, S.; López-Benítez, M.: Improved likelihood ratio statistic-based cooperative spectrum sensing for cognitive radio. IET Commun. **14**(11), 101–112 (2020)
6. Qingqing, W.; Rui, Z.: Beamforming optimization for intelligent reflecting surface with discrete phase shifts. ICASSP (2019)
7. Hongliang, Z.; Boya, D.; Lingyang, S.; Zhu, H.: Reconfigurable intelligent surfaces assisted communications with limited phase shifts: how many phase shifts are enough? IEEE Trans. Veh. Technol. **69**(4), 4498–4502 (2020)
8. Ertugrul, B.; Di Renzo, M.; De Rosny, J.; Debbah, M.; Alouini, M.S.; Zhang, R.: Wireless communications through reconfigurable intelligent surfaces. IEEE Access **7**(1), 116753–116773 (2019)
9. Qingqing, W.; Rui, Z.: Towards smart and reconfigurable environment: intelligent reflecting surface aided wireless network. IEEE Commun. Mag. **58**(1), 106–112 (2020)
10. Ertugrul, B.: Reconfigurable intelligent surface-based index modulation: a new beyond mimo paradigm for 6G. IEEE Trans. Commun. **68**(5), 3187–3196 (2020)
11. Di Renzo M.: 6G wireless: wireless networks empowered by reconfigurable intelligent surfaces. In: Proceedings of the 2019 25th Asia-Pacific Conference on Communications (APCC)
12. Chongwen, H.; Zappone, A.; Alexandropoulos, G.; Debbah, M.; Yuen, C.: Reconfigurable intelligent surfaces for energy efficiency in wireless communication. IEEE Trans. Wireless Commun. **18**(8), 4157–4170 (2019)
13. Huayan, G.; Ying-Chang, L.; Jie, C.; Larsson, E.: Weighted sum-rate maximization for reconfigurable intelligent surface aided wireless networks. IEEE Trans. Wireless Commun. **19**(5), 3064–3076 (2020)
14. Alexandropoulos G.; Vlachos E.: A hardware architecture for reconfigurable intelligent surfaces with minimal active elements for explicit channel estimation. ICASSP IEEE International Conference on Acoustics, Speech and Signal Processing (ICASSP) (2020)
15. Thirumavalavan V.C.; Jayaraman T.S.: BER analysis of reconfigurable intelligent surface assisted downlink power domain NOMA system. In: Proceedings of the 2020 International Conference on COMmunication Systems and NETworkS (COMSNETS) (2020)
16. Pradhan, C.; Li, A.; Song, L.; Vucetic, B.; Li, Y.: Hybrid precoding design for reconfigurable intelligent surface aided mmWave communication systems. IEEE Wireless Commun. Lett. **9**(7), 1041–1045 (2020)
17. Ying, K.; Gao, Z.; Lyu, S.; Wu, Y.; Wang, H.; Alouini, M.S.: GMD-based hybrid beamforming for large reconfigurable intelligent surface assisted millimeter-wave massive MIMO. IEEE Access **8**(1), 19530–19539 (2020)
18. Yang, L.; Guo, W.; Ansari, I.S.: Mixed dual-hop FSO-RF communication systems through reconfigurable intelligent surface. IEEE Commun. Lett. **24**(7), 1558–1562 (2020)
19. Di, B.; Zhang, H.; Li, L.; Song, L.; Li, Y.; Han, Z.: Practical hybrid beamforming with finite-resolution phase shifters for reconfigurable intelligent surface based multi-user communications. IEEE Trans. Veh. Technol. **69**(4), 4565–4570 (2020)
20. Zhao, W.; Wang, G.; Atapattu, S.; Tsiftsis, T.A.; Tellambura, C.: Is backscatter link stronger than direct link in reconfigurable intelligent surface-assisted system? IEEE Commun. Lett. **24**(6), 1342–1346 (2020)
21. Nadeem, Q.; Kammoun, A.; Chaaban, A.; Debbah, M.; Alouini, M.S.: Asymptotic max–min SINR analysis of reconfigurable intelligent surface assisted miso systems. IEEE Trans. Wireless Commun. **19**(12), 7748–7764 (2020)
22. Dai, L.; Wang, B.; Wang, M.; Yang, X.; Tan, J.; Shuangkaisheng, B.; Shenheng, X.; Fan, Y.; Zhi, C.; Di Renzo, M.; Chan-Byoung, C.; Hanzo, L.: Reconfigurable intelligent surface-based wireless communications: antenna design, prototyping, and experimental results. IEEE Access **8**(1), 45913–45923 (2020)
23. Makarfi, A.U.; Kharel, R.; Rabie, K.M.; Kaiwartya, O.; Li, X.; Do, D.T.: Reconfigurable intelligent surfaces based cognitive radio networks. IEEE Wireless Communications and Networking Conference Workshops (2021)
24. He, J.; Kaiqiang, Y.; Yong, Z.; Yuanming, S.: Reconfigurable intelligent surface enhanced cognitive radio networks. In: IEEE 92nd Vehicular Technology Conference (VTC-Fall) (2020)
25. Jie, Y.; Ying-Chang, L.; Jingon, J.; Gang, F.; Larsson, E. G.: Intelligent reflecting surface (IRS)-enhanced cognitive radio system. ICC, IEEE International Conference on Communications (ICC) (2020)
26. Jie, Y.; Ying-Chang, L.; Jingon, J.; Gang, F.; Larsson, E.G.: Intelligent reflecting surface-assisted cognitive radio system. IEEE Trans. Commun. **69**(1), 675–687 (2021)
27. Lei, Z.; Yu, W.; Weige, T.; Ziyan, J.; Tiecheng, S.; Cunhua, P.: Intelligent reflecting surface aided MIMO cognitive radio systems. IEEE Trans. Veh. Technol. **69**(10), 11445–11457 (2020)
28. Dongfang, X.; Xianghao, Y.; Robert, S.: Resource allocation for intelligent reflecting surface-assisted cognitive radio networks. In: IEEE 21st International Workshop on Signal Processing Advances in Wireless Communications (SPAWC) (2020)
29. Fatemeh, Z.; Mohammad, R.S.; Qingqing, W.: Vertical beamforming in intelligent reflecting surface-aided cognitive radio networks. IEEE Wireless Communications Letters, Early access article (2021)
30. Lei, Z.; Cunhua, P.; Yu, W.; Hong, R.; Kezhi, W.; Arumugam, N.: Robust beamforming optimization for intelligent reflecting surface aided cognitive radio networks. GLOBECOM, IEEE Global Communications Conference (2020)
31. Dong, L.; Hui-Ming, W.; Haitao, X.: Secure cognitive radio communication via intelligent reflecting surface. IEEE Trans. Commun. **69**(7), 4678–4690 (2021)

32. Limeng, D.; Hui-Ming, W.; Haitao, X.; Jiale, B.: Secure intelligent reflecting surface assisted MIMO cognitive radio transmission. Presented at the (2021)
33. Proakis, J.: Digital Communications, 5th edn Mac Graw-Hill, New York (2007)
34. Alhamad, R.; Boujemaa, H.: Cooperative spectrum sensing with energy harvesting for Nakagami fading channels. Int. J. Sens. Netw. IJSNET **33**(1), 1–7 (2020)
35. Xi, Y.; Burr, A.; Wei, J.B.; Grace, D.: A general upper bound to evaluate packet error rate over quasi-static fading channels. IEEE Trans. Wireless Commun. **10**(5), 1373–1377 (2011)